International Journal of Micro Air Vehicles

Article

International Journal of Micro Air Vehicles
2017, Vol. 9(4) 253–269

DOI: 10.1177/1756829316682148
journals.sagepub.com/home/mav

SAGE

Design and analysis of the link mechanism for the flapping wing MAV using flexible multi-body dynamic analysis

JaeHyeok Jeon, Haeseong Cho, Younghwan Kim, JunHee Lee, DuHyun Gong, SangJoon Shin and Chongam Kim

Abstract

Recently, there has been an increase in the research on flapping wing vehicles which mimic biological motions. One result has been the flapping wing micro-aerial vehicle. In this paper, the design requirements for flapping wing micro-aerial vehicles were established through an analysis with the unsteady blade element theory. Then, based on the flapping wing micro-aerial vehicle design requirements, a flapping wing mechanism using a pair of six-bar linkage was devised. Moreover, several candidates for the present mechanism were analyzed using a flexible multi-body dynamic analysis to ensure the structural appropriateness of the mechanism. By completing such procedures, the performance of the present mechanism could be evaluated. A detailed design was then conducted. The structural analysis of the present mechanism was conducted regarding its flapping operation in a vacuum. The resulting von Mises stresses in the linkage were targeted to be smaller than the yield stresses of the chosen material. Next, additional details of the design and an experiment on the present flapping wing micro-aerial vehicle were conducted to validate its performance.

Keywords

Flapping wing MAV, flexible multi-body dynamic analysis, MAV design, MAV manufacture, 6-bar linkage mechanism

Date received: 18 July 2016; accepted: 29 August 2016

Introduction

Flapping wing micro-aerial vehicles (FWMAVs) have developed greatly over the last few decades, with relevant research showing significant growth. The design of a FWMAV can be conducted through an examination of natural flyers by mimicking their biological features. Natural flyers are examined for this purpose because they can hover, unlike a fixed-wing MAV. They are also more efficient than a rotary-wing MAV.[1] Using these advantages, the FWMAV is capable of conducting various tasks. Specifically, an insect-mimicking FWMAV operates in a low-Reynolds-number aerodynamic environment. Its flight control is implemented by the unique mechanism of multi-wing operation at a high flapping frequency and with a large flapping amplitude. As a result, FWMAVs may contain complicated mechanisms in order to implement such operations. Moreover, FWMAVs do not have tail wings. To control their fuselage, FWMAVs are required to use simultaneously both sides of flapping wing motions. Currently, many methods for more stable flight are being investigated. George et al.[2] developed a differentially driven flapping wing mechanism. In their examination, the trajectory optimization and load analysis were conducted. Moreover, a number of the previous MAVs were described in detail in their literature.

Some examples of the flapping mechanisms are as follows. One of those is the Nano Hummingbird[3] developed by AeroVironment, Inc. It is one of the most advanced vehicles, able to hover and operate in backward and forward flight. Its driving component includes strings which allows both wings to move simultaneously. Robobee,[4] developed at Harvard

Department of Mechanical and Aerospace Engineering, Seoul National University, Seoul, Korea

Corresponding author:
SangJoon Shin, Department of Mechanical and Aerospace Engineering, Seoul National University, Seoul 151-744, Korea.
Email: ssjoon@snu.ac.kr

University, is the smallest vehicle to use a piezoelectric actuator as its driving component. In addition, a few vehicles, such as the Golden Snitch[5,6] by Tamkang University and BionicOpter[7] by Festo, adopt conventional mechanical linkages for flapping wing movements. However, Golden Snitch has slightly longer wing span than it should be in the general definition of MAVs. Also, it is not appropriate for insect-mimicking flight, a tailless flight. Insect-mimicking FWMAVs must generate control forces, i.e. pitching, yawing, and rolling moments, with both wings flapping periodically. This suggests that the aerodynamic forces generated on each side of the wings will become unbalanced momentarily.[8] Based on such physical characteristics, several control mechanisms are available. Nano Hummingbird uses a wing twisting mechanism.[3] This mechanism changes the membrane shape by modifying the trailing edge to generate different lift on each wing. BionicOpter[7] by Festo modifies the direction of the flapping plane of each wing to generate unbalanced aerodynamic force. On the other hand, the robotic hummingbird by Bruxelles University varies the position of its kinematic joints to change the flapping angle and offset of the flapping plane.[8] However, several of the mechanisms mentioned above require a considerable amount of space owing to their large driving or control components. Moreover, modifying the trailing edge requires experimental verification and an aerodynamics database to induce reasonable performance. Significant collaboration with analytical design teams is also required during the design process.

In this paper, a six-bar linkage mechanism is suggested. This mechanism requires a relatively small driving component through two separate kinematical steps relying on its six-bar linkage characteristics. The wing motions for the flight control are simply generated from a small position change of the joints. Additionally, kinematics and structural analyses may provide a more realistic result with regard to the design. With a fundamental analysis using the unsteady blade element theory (UBET),[9] certain design requirements will be established. The design of the flapping mechanism using the present mechanical linkage will then be realized. In order to predict the structural reliability of the present mechanism, a flexible multi-body dynamic analysis using RecurDyn will be performed. In the present mechanism, the wings are connected to the mechanical linkage and are not directly connected to the joint. Thus, it is possible to obtain a sufficient flapping amplitude and adjust the flapping kinematic by varying the joint location. Currently, the actuation mechanism which steers the joints is not yet included. Using the results of the structural analysis, a detailed design of the present control actuation mechanism will be devised. Finally, an experiment on the present mechanism will be conducted to validate the performance, specifically by examining the control forces, flapping frequency, and flapping angle.

Design procedure

In previous studies,[3–5,7] a kinematic analysis using multi-body dynamics was not utilized during the design procedure of FWMAVs, although it was capable of providing a significantly precise design result. In this paper, a design procedure which utilizes a multi-body dynamics analysis is introduced, as shown in Figure 1. The design procedure is divided into nine stages, from

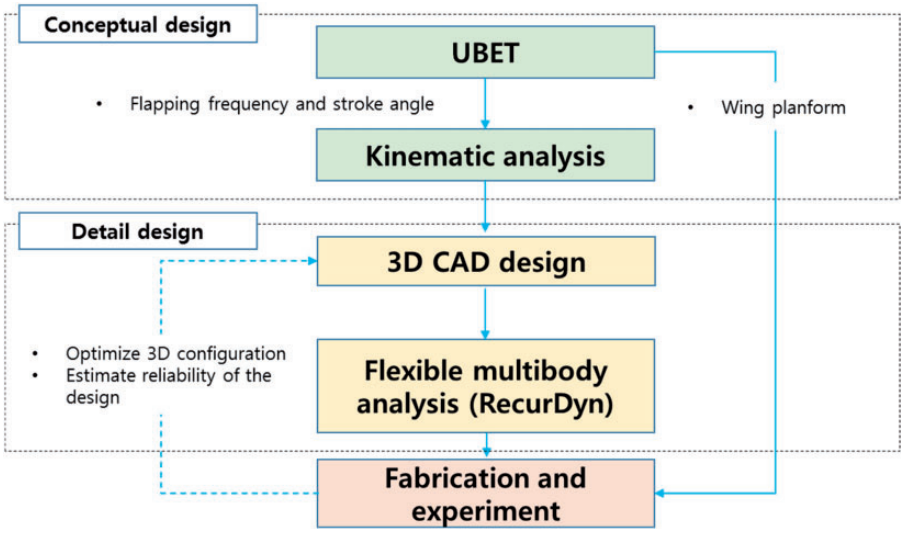

Figure 1. Diagram of the present design procedure.

the design requirement to the design completion. The first stage is the design requirements, including weight and span limits. To uplift the weight, appropriate thrust is needed. The flapping angle and frequency for the thrust are deduced through the second stage, UBET. Third, a conceptual design is conducted to convert the rotation of the motor to the flapping motion. In this paper, the main mechanism is the six-bar linkage mechanism. The next stage is the kinematic analysis. In this stage, the design parameters such as the link lengths and joint positions are determined with regard to the design requirements. The developed idea is then embodied in a three-dimensional CAD shape before the flexible multi-body dynamic analysis is applied. With this three-dimensional CAD design, a flexible multi-body dynamic analysis utilizing the commercial software RecurDyn[10] is conducted to examine the possibility of fabrication via an understanding of the design parameters and execution faults. The sixth stage is the component selection. Commercially available components, such as motor and gears, are purchased, and other components are processed with regard to the result of FMBD. The next stage includes the fabrication and experimental processes. Subsequently, the performance of the conceptual design is evaluated to determine whether to go to the next stage or return to the previous stage. At this stage, the conceptual design is realized by applying the actual materials, and performance of the FWMAV is evaluated using a test bed which takes into account the aerodynamic force, flapping conditions, and design requirements. In the event problems are found, modification and supplementation will be required. Through this procedure, the flapping mechanisms will be optimized for robustness.

Design requirements

In this section, the preliminary design requirements will be established. First, the wing span was determined to be 150 mm by referring to the definition of a general FWMAV. The gross weight was then assumed to be 20 g by considering off-the-shelf products, such as an electric motor, a servo motor, a joint pin, and others. Finally, appropriate flapping amplitude and actuation frequency which would create sufficient lift were estimated using UBET prediction.[8] UBET refers to an unsteady blade element theory which is based on quasi-steady aerodynamics. In the present UBET analysis, the wing mass and center of gravity were set to 0.1 g and 0.1%, respectively, along the chord length in each case. In addition, three types of wing planforms were considered, i.e. rectangular, elliptic, and insect-like wings. The configuration of the wings is illustrated in Figure 2.

According to the predictions by the UBET analysis, the flapping stroke amplitude and actuation frequency need to be greater than 150° and 37 Hz, respectively, to obtain sufficient lift for a gross weight of 20 g. Table 1 summarizes the results with respect to these wing planforms. Except for the elliptic planform, the rectangular and insect-like planforms were predicted to provide over the gross weight, 20 g. The rectangular planform provides larger wing loading (thrust/area of single wing) than the others do, as was suggested by the present UBET prediction. However, the wing planform was determined to employ the insect-like planform to obey the trends in the previous studies.[11] This is because an insect-like planform is beneficial for lift production. Finally, the fundamental design requirements for the present FWMAV were then determined. These results are summarized in Table 2.

Table 1. UBET results for flapping amplitude of 150° and frequency of 37 Hz.

Planform	Square	Elliptic	Insect
Thrust (N)	0.24	0.19	0.20
Area of a single wing (mm^2)	1761.3	1584.5	1627.2
Thrust/area of a single wing (N/m^2)	67.13	60.10	61.54

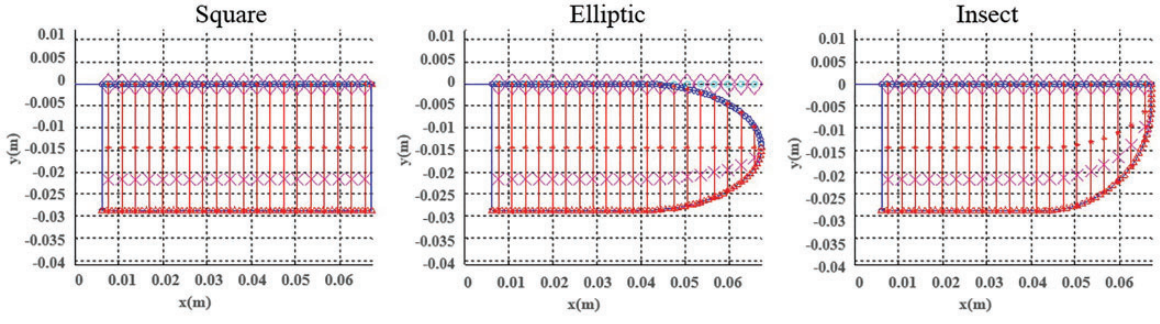

Figure 2. Three-wing planform configurations.

Table 2. Preliminary design requirements for the present FWMAV.

Wingspan	Weight	Flapping amplitude	Flapping frequency
150 mm	20 g	150°	37 Hz

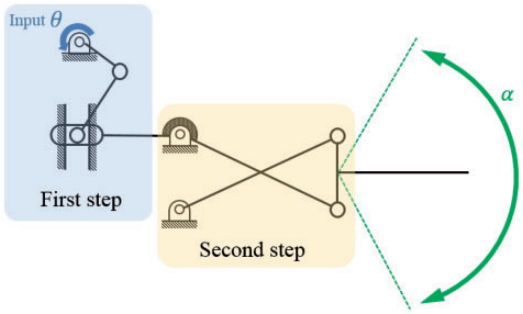

Figure 3. Diagram of the two-step flapping mechanism.

Flapping mechanism

The present driving components consist of a DC motor, gears, and linkages. To generate the flapping motion, the revolution of the motor needs to be transformed into reciprocating angular motion. In the present mechanism, a certain type of six-bar linkage was utilized to provide a combination of two separate types of kinematics. One mechanism close to the input link is the crank-slider mechanism, which consists of a four-bar linkage and which creates back and forth motion. However, the crank-slider mechanism is an asymmetric mechanism, which creates a difference slider speed between the forward and returning stroke, known as a quick return mechanism. To reduce the asymmetric characteristic of the crank-slider mechanism, an alternate step mechanism is required. The second step close to the wing consists of a crossed four-bar link which compensates for the asymmetry of the initial four-bar linkage. Moreover, this second step is capable of amplifying the crank-slider motion, as depicted in Figure 3. This suggests that the final flapping angle can be increased further. Using such a mechanism, it is possible to minimize the dimensions of the driving components and create the desired control capability at the same time. In this section, a parametric design was conducted to satisfy the design requirements acquired in the Design requirements section.

Kinematics of the present flapping mechanism

In this section, the formulation for the present six-bar linkage is presented. It was in order to estimate the appropriate length of linkages regarding the required flapping motion, determined in the previous section. Moreover, the formulation was applied to design the control mechanism (see the Control mechanism section). As described at the beginning of this section, the present six-bar linkage uses the following two steps to create the flapping motion. Here, the kinematics of the linkages is analyzed in detail to predict the motion. The first mechanism of the present six-bar linkage can be expressed by taking the geometry and angular motion of the frames into account, as follows.

$$\theta_4 = \tan^{-1}\left(\frac{\sqrt{r_3^2 - (r_2\sin\theta_1)^2} + r_2\cos\theta_1 - r_1}{r_4}\right) \quad (1)$$

Here, θ_1 is the input angle by the motor rotation, and θ_4 is the initial angle of the second mechanism. The first stage in the crank-slider mechanism is capable of generating rotation at point $P_4 \pm 5^\circ$ by the rotation of the motor. A joint rotation in the second mechanism can then be derived from the equation of the four-bar linkage. The resulting formulas can be expressed as follows.

$$\theta_6 = \cos^{-1}\left(\frac{C}{\sqrt{A^2 + B^2}}\right) + \tan^{-1}\left(\frac{B}{A}\right) \quad (2)$$

$$\theta_5 = \sin^{-1}\left(\frac{r_6\sin\theta_4 - r_8\sin\theta_6}{r_7}\right) \quad (3)$$

$$\theta_7 = \cos^{-1}\left(\frac{r_6^2 + r_7^2 - \left(\sqrt{(-r_5 + r_8\cos\theta_6)^2 + (r_8\sin\theta_6)^2}\right)^2}{2r_6r_7}\right) \quad (4)$$

Here, A, B and C are determined by the following geometrical consideration for the linkages.

$$\begin{aligned} A &= -2(r_6r_8\cos\theta_4) + 2r_5r_8 \\ B &= -2r_6r_8\sin\theta_4 \\ C &= r_7^2 - r_6^2 - r_8^2 - r_5^2 - 2r_5r_6\cos\theta_4 \end{aligned} \quad (5)$$

By completing these procedures, an accurate prediction of the kinematics of the linkages becomes possible. The flapping stroke amplitude in the present mechanism is obtained by the complicated linkage motion shown in Figure 4. The bending angle of the linkage r_8 is expressed as γ. The first mechanism made of the crank slider is capable of transforming the motor rotation into a straight-line motion. However, such motion output is not symmetric at this point, as mentioned earlier. The second mechanism consists of the four-bar linkage.

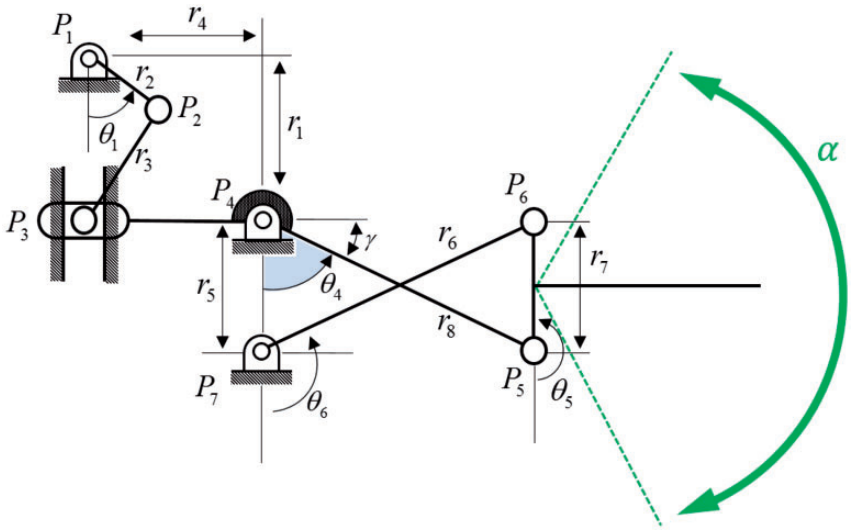

Figure 4. Kinematic scheme of the present six-bar linkage.

Table 3. Dimensions of the linkage components.

Linkage	r_1	r_2	r_3	r_4	r_5	r_6	r_7	r_8
Length (mm)	6.91	3.75	7.86	3.5	3.5	8	4.5	8

It increases the amplitude of the motion obtained by the first mechanism. The combination of these two stages generates the total flapping amplitude. Thus, the flapping amplitude in this mechanism is defined by the sum of the joint rotation at point P_4 in the first step and at point P_5 in the second step.

The dimension of the driving components was satisfactory with regard to the design requirements. The resulting dimensions of each linkage were also determined. The relevant values are summarized in Table 3.

Control mechanism

Conceptual design of the control mechanism

In this section, a control mechanism using the aforementioned linkage mechanism is presented. In an insect-mimicking FWMAV, the aerodynamic difference between the two wings may introduce unbalanced moment. Therefore, the vehicle is required to have the capability for changing the wings' position. There are two major control mechanisms. One is the trailing edge control (TEC) mechanism which is called as wing twist modulation in Nano Hummingbird.[3] This mechanism changes the angle of attack or camber of the wings by steering the trailing edge. The other is the flapping plane control mechanism. This mechanism is combined with the main flapping mechanism. It changes the flapping amplitude or tilts the flapping plane forward or backward. The present design employed the flapping plane control mechanism by integrating both flapping and control mechanisms. Such compact combination will be beneficial for the design of a small-sized MAV when compared to the trailing edge control mechanism. Figure 5 illustrates the right-hand side of the wing and describes the joint motion along the θ and r directions at P_7. This joint with two degrees of freedom can modify the flapping amplitude, α, and rotation of the flapping plane, β, which is the alteration of the center line of the flapping plane.

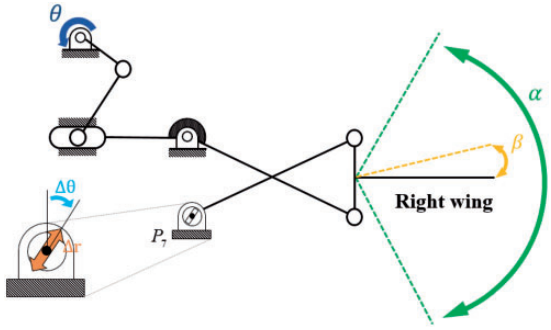

Figure 5. Kinematic diagram of the moving joint on the right wing.

The two-dimensional multi-body dynamics analysis using RecurDyn, based on rigid body assumption, was conducted to estimate the influence with respect to the position of Joint P_7. Figure 6 shows the variation of the flapping amplitude, α, with respect to the position of Joint P_7 according to θ and r directions. Figure 7 shows the variation regarding the rotation angle of the flapping plane with respect to the position of Joint P_7.

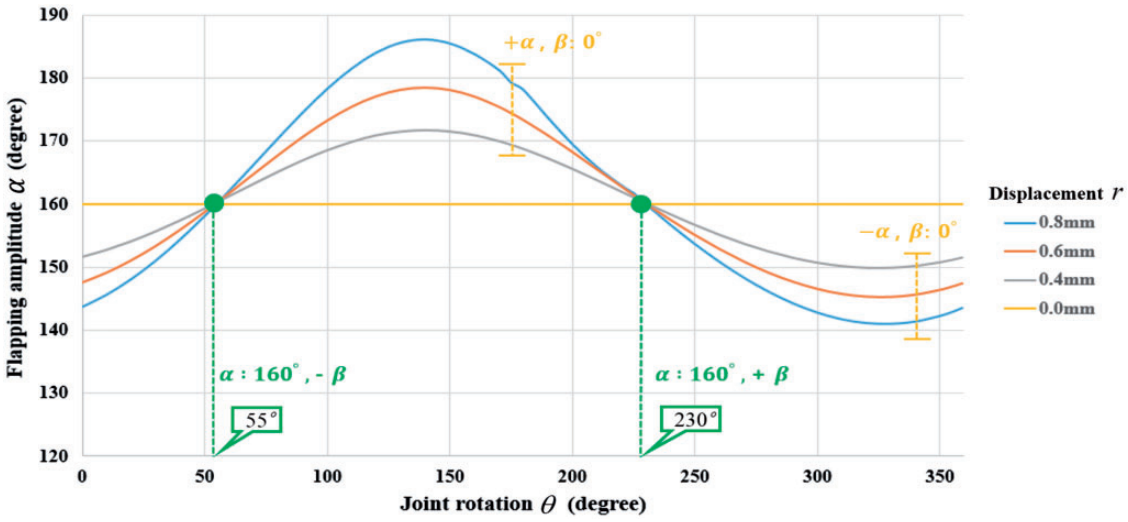

Figure 6. The trajectory curve of the flapping amplitude.

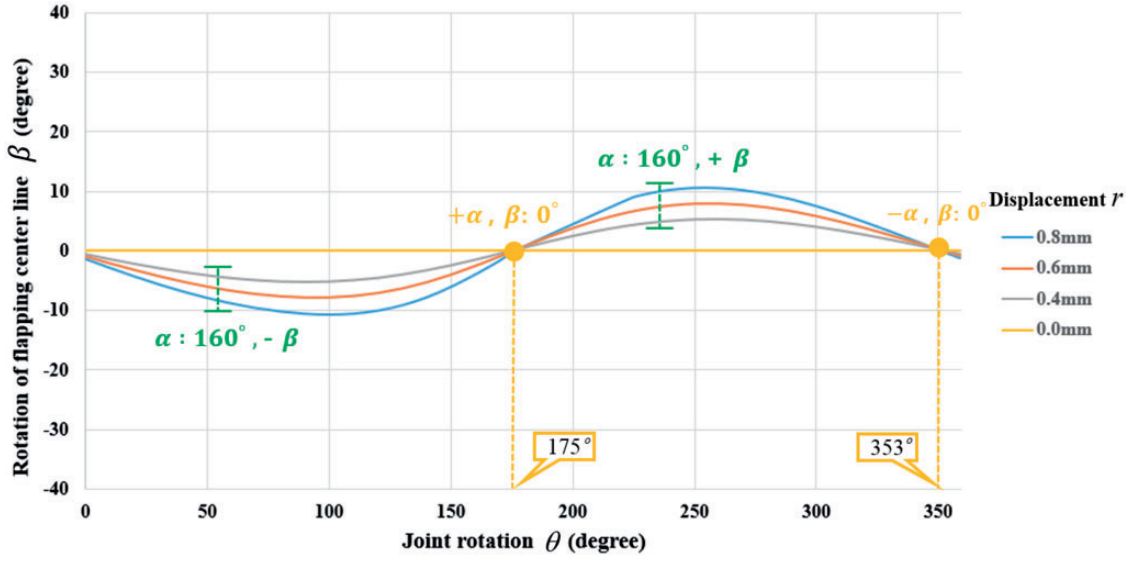

Figure 7. Trajectory of rotation of the flapping center line.

When the joint rotation angle θ is either 55° or 230°, the flapping stroke amplitude will maintain its neutral flapping amplitude of 160°, as depicted in Figure 6. However, the rotation of the flapping plane is varied to either a positive or negative value, as depicted in Figure 7. This suggests that the flapping plane will rotate by the amount β with a constant flapping amplitude, α, of 160°. This result is obtained regardless of the joint displacement r. By the present mechanism, the flapping stroke plane will be varied in either the clockwise or counter-clockwise direction, while it maintains the same flapping stroke amplitude. By applying the present mechanism for each wing, it will be possible to generate the yawing moment of the vehicle. Moreover, when the joint rotation angle θ is either 175° or 353°, the rotation of the flapping center line will maintain its neutral position $\beta = 0°$ regardless of the joint displacement, r, as shown in Figure 7. Simultaneously, the flapping stroke amplitude will take either a positive or negative value according to the joint displacement r, as shown in Figure 7. By using this mechanism, it will be possible to either increase or decrease the flapping stroke amplitude. This motion induces differences in the force acting along the axis perpendicular to the flapping plane. Thus, it is possible to generate rolling and pitching

moment of the vehicle. In the present control mechanism, the joint displacement, r, was set to be 0.8 mm, leading to the maximum variations in the stroke amplitude and rotation of the flapping plane. As a result, optimized control points were obtained. Values of the relevant variations with respect to the control points are summarized in Table 4. Geometric configuration of the resulting control points is illustrated in Figure 8. In the next section, detailed idea which brings the aerodynamic moment under the configuration of the present control points will be described. Then, the following sections regarding three-dimensional numerical analysis (Three-dimensional design section) and experiment (Fabrication and experiment section) will discuss about the reliability of the present mechanism.

Pitching, rolling, and yawing motion

In order to generate the pitching moment, both wings will retain a flapping amplitude, α, of 160°. In addition, the center line of the flapping plane is rotated by the same magnitude, β. The relevant situation is illustrated in Figure 9. In the figure, the aerodynamic center of both wings is segregated from the center of gravity of the vehicle. This causes the nose to move up or down.

Table 4. Values of the resulting control points.

Control points	Flapping amplitude, α	Rotation of the flapping plane, β
N (neutral)	160°	0°
α_N	160°–20°	0°
α_P	160° + 20°	0°
β_N	160°	−10°
β_P	160°	+10°

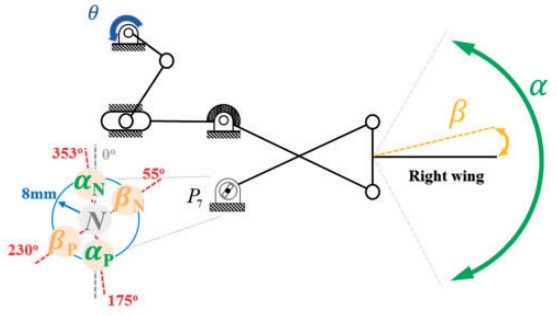

Figure 8. Configuration of the joint positions related with the control points.

Next, yawing moment can be generated by the unsymmetrical motion of the wings. Both wings retain a flapping amplitude, α, of 160° and each flapping plane is rotated in the reverse direction, as shown in Figure 10. Under this condition, the aerodynamic center of each wing will be rotated in a direction identical to that of the original aerodynamic center location. This will also cause the nose to move up or down, as shown in Figure 10.

The last moment to be considered is the rolling moment. To create the rolling moment, each wing must have a different flapping stroke amplitude. Furthermore, both sides of the wings have a neutral position on the center line of the flapping plane, $\beta = 0°$. For example, as depicted in Figure 11, the left-hand wing can create a greater amount of lift than the right-hand wing.

As a result, conceptual design of the control mechanism using the present link mechanism was conducted. Moreover, feasible applications for generating the aerodynamic moments were described. In the next section, three-dimensional implementation and the analysis of the present link mechanism will be presented.

Three-dimensional design

In this section, three-dimensional design of the aforementioned mechanisms was conducted for flexible multi-body dynamics. All the predictions were simulated using the flexible multi-body dynamic analysis program, RecurDyn. In this procedure, the play between the joints and linkages are not considered. First, three-dimensional implementation using CAD was conducted, and prediction regarding the flapping mechanism was conducted. The relevant comparison of the quasi-steady response induced by the control mechanism is then described in the following section. Moreover, stress prediction of the present mechanism was conducted in order to estimate the relevant thickness of each linkage.

Flapping mechanism

Before the flexible multi-body dynamic analysis of the present mechanism is applied, a three-dimensional model was created. Based on the kinematic analysis, the three-dimensional flapping mechanism was created, as shown in Figure 12. It consists of rivets, a DC motor (DiDEL MK07-08), gears, brass bearings, and the fuselage frame (epoxy glass laminate). In its three-dimensional configuration, multiple numbers of yellow circular-sectional shaft pins represent the hinge fixed on the fuselage frame, which withstands the bulk of the load generated by the flapping motion. The motor and gear box are located below the present

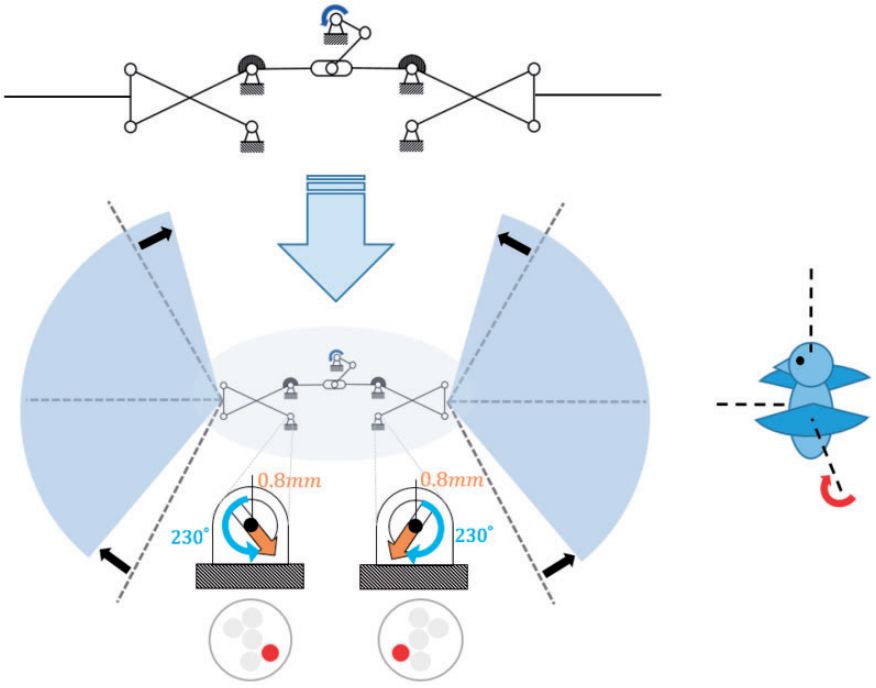

Figure 9. Joint position for the pitching motion.

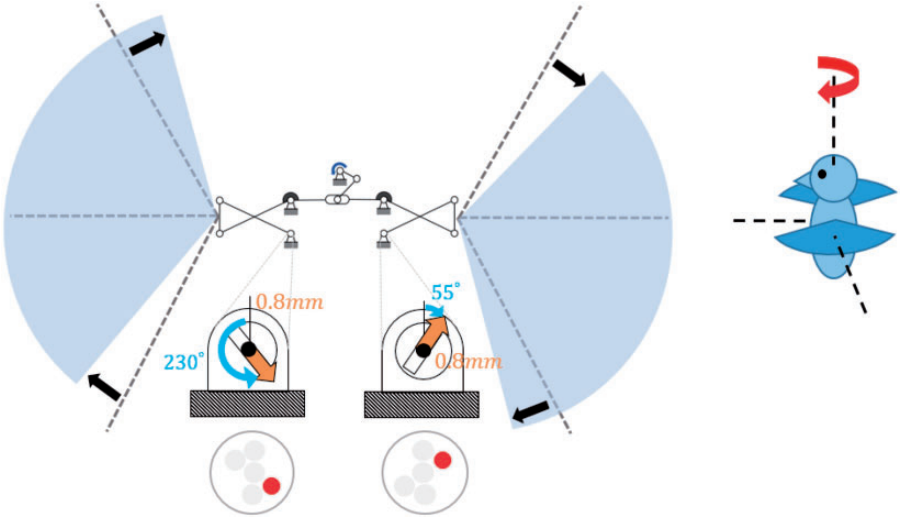

Figure 10. Joint position for the yawing motion.

mechanism. These components are located between the two wings considering the center of gravity of the entire vehicle. The linkages, which are similar to tongs, are capable of holding the wing batten connected to the wing membrane. The material of the present fuselage frame is an epoxy glass laminate, which is light and structurally strong. The flapping amplitude of the present three-dimensional configuration was estimated in the flexible multi-body dynamic analysis. To evaluate the accuracy of the kinematic solution, the analysis was performed while assuming only rigid-body rotational motion. As shown in Figure 13, the results obtained with this mechanism showed an upstroke and downstroke with symmetric amplitudes at a constant time step. Thus, the stroke motion was relatively well matched by the sinusoidal curve. Moreover, the flapping amplitude was estimated to be sufficient, at approximately 160°.

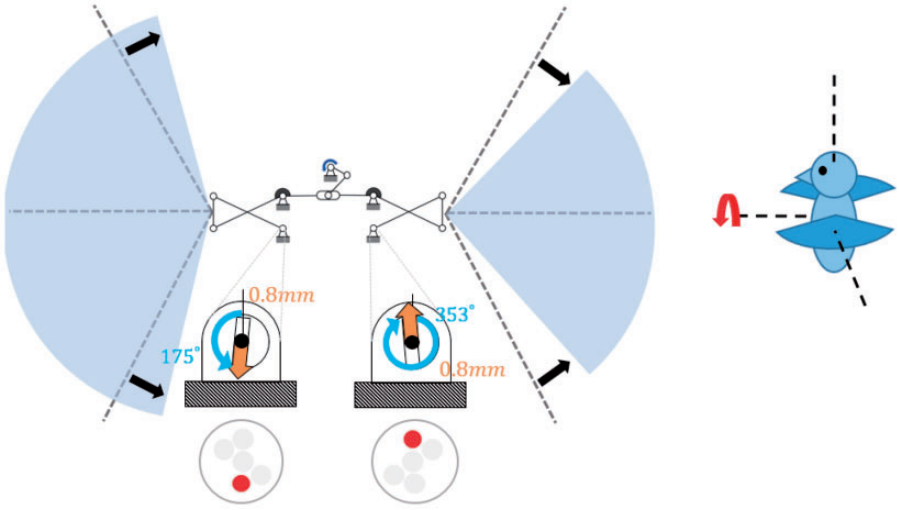

Figure 11. Joint position for the rolling motion.

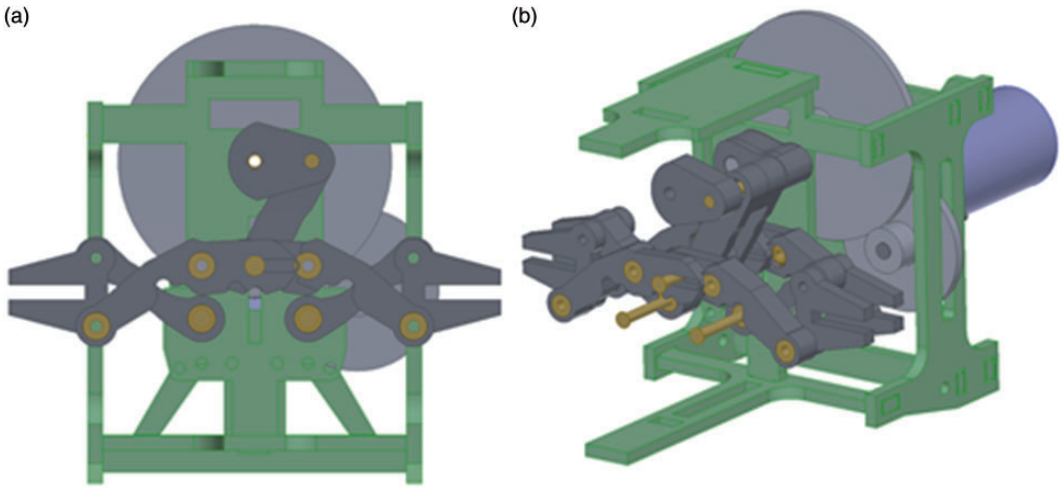

Figure 12. Three-dimensional CAD drawings of the flapping mechanism. (a) Front view and (b) isometric view.

Control mechanism

As shown in Figure 14, the control mechanism was designed to generate joint motion by obeying specified requirements in the Control mechanism section. In the present three-dimensional configuration, a simple rotating and pulling mechanism was utilized to simplify the fabrication procedure. To analyze the control mechanism, a multi-body dynamic analysis by RecurDyn was used. In Figure 15(a), the components in blue were devised to control the θ rotation while those in brown are devised to control the r direction, as depicted in Figure 15(b).

First, the joint motion was prescribed to change the flapping stroke amplitude α. Recalling the control points depicted in Figure 8, the joint position was varied. When the joint was located at the control point, α_P, the flapping amplitude was increased. On the other hand, when the joint was located at the control point, α_N, the flapping amplitude was decreased. Figure 16 shows a steady-state response of the wing stroke when the joint is at the control point, α_N.

In order to generate the yawing motion, the flapping amplitude was held constant but the flapping plane should be rotated. Therefore, the joint was located at the control point, β_P. The flapping plane was rotated by approximately $+8^\circ$, while maintaining the flapping amplitude. When the joint was located at the control point, β_N, the flapping plane was rotated in the negative direction while maintaining the same flapping amplitude.

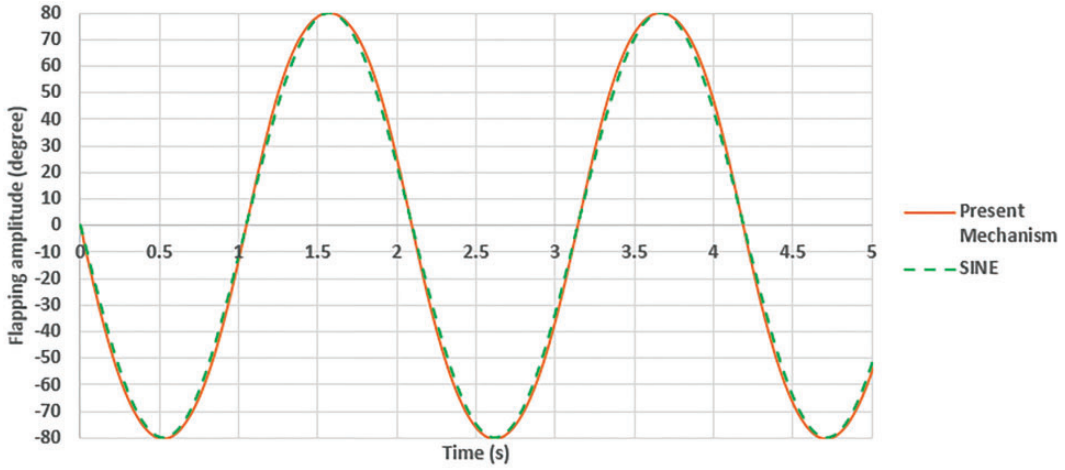

Figure 13. Rotation angle result of the flapping wing mechanism.

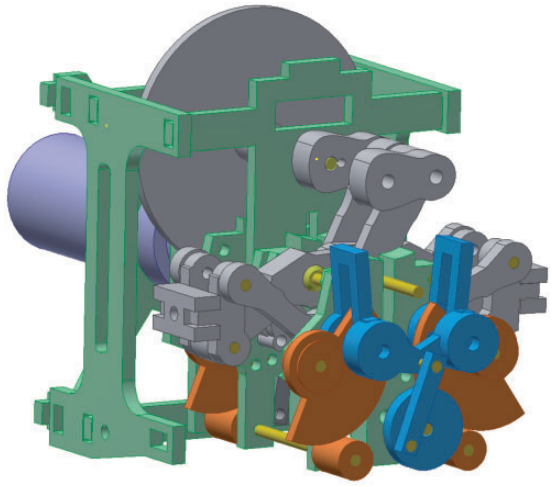

Figure 14. Three-dimensional CAD drawings of the control mechanism.

The relevant result when the joint is at the control point, β_N, is illustrated in Figure 17. As a result, the three-dimensional implementation of the preliminary control mechanism concept was successfully completed.

Stress prediction using flexible multi-body dynamic analysis

After the verification of the flapping and control mechanisms was completed, a flexible multi-body dynamic analysis was conducted to predict the stress induced in the linkages. In this analysis, the flapping frequency was set to be 37 Hz, which was the design requirement. From the prediction on the stress in the linkages, the relevant stiffness of each link was determined by adjusting the thickness of the link. The thickness of all the linkages was determined to be the same in the initial design. However, the maximum stress induced in Links 1 and 5 had been predicted to be larger than the yield strength of the constituent material, i.e. epoxy glass laminate. Epoxy glass laminate has a yield strength of 870 MPa. After the thickness of Links 1 and 5 was adjusted, the analysis was re-conducted. The relevant result is illustrated in Figure 18. The maximum von Mises stress was predicted to be 291 MPa, as shown in red in Figure 18. By comparing the maximum predicted stress with the material yield strength, the safety of the proposed mechanism was proved. The margin of safety was 67%. However, in the flexible analysis, only flapping operation in a vacuum was considered. In order to obtain a more realistic prediction, the aerodynamic loads induced by the flapping motion will be predicted and added.

Fabrication and experiment

Fabrication

Figure 20 shows the fabricated prototype. To satisfy the design requirement weight, the fuselage was made of epoxy glass laminate, a relatively lightweight material with high solidity compared to other materials. Here, 1 mm and 2 mm plates of epoxy glass laminate were prepared by a CNC cutting machine for the fuselage components. In all of the connected joints, the brass bearings having a diameter of 0.8 mm were used to maintain the accuracy and minimize the rotational friction. The motor that was selected for use was the MK07-08 by DiDEL. It can generate 0.37 N-mm of torque at 40,000 r/min with no load condition at 4.5 V. A nine-tooth pinion, a 12/36-tooth gear, and a

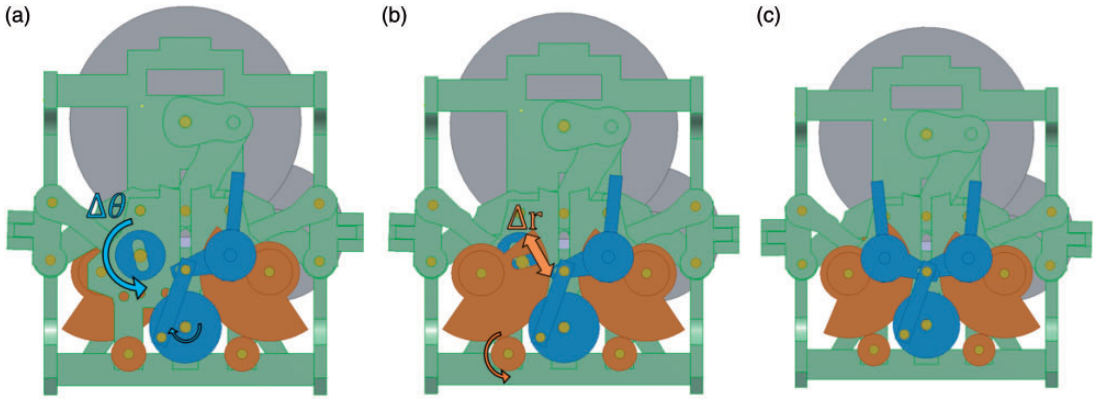

Figure 15. Three-dimensional CAD drawings of the control mechanism: (a) θ - Motion, (b) r - Motion and (c) Front view.

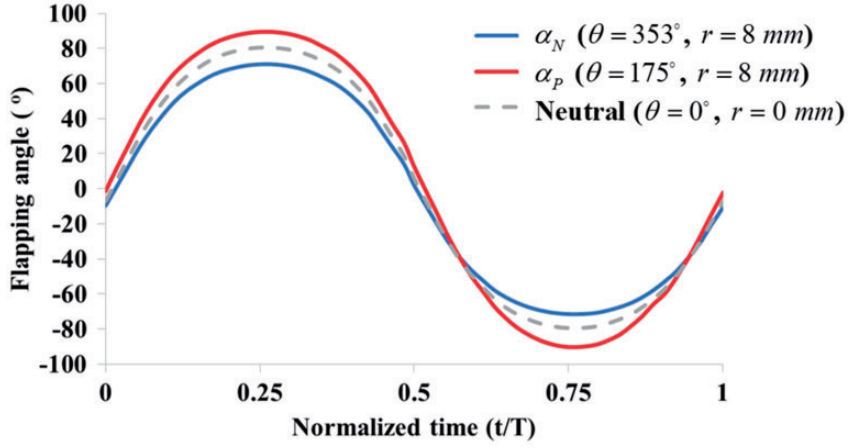

Figure 16. Flapping amplitude variation according to the joint motion of the θ and r directions for the rolling motion.

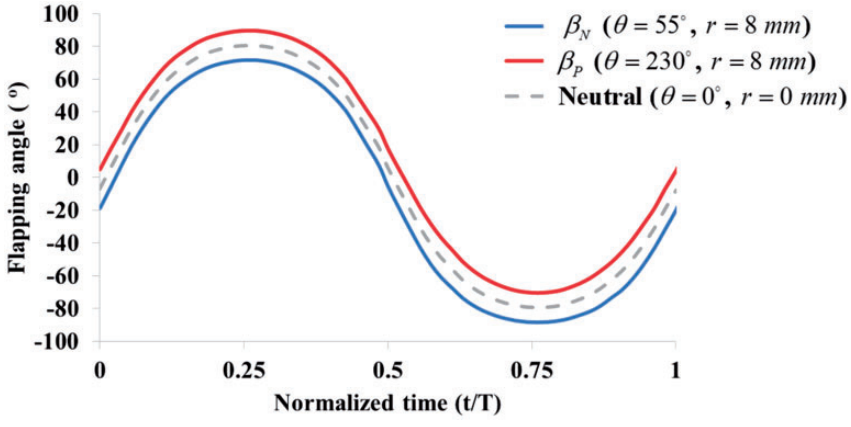

Figure 17. Flapping amplitude variation according to the joint motion of the θ and r directions for the yawing motion.

12/60-tooth gear by DiDEL were used to obtain a 20:1 gear ratio. Using this gear ratio, the motor will provide 7.4 N-mm of torque at 2,400 r/min with no load condition at 3.5 V. This condition was selected considering the predicted flapping frequency of 37 Hz. Consequently, the external dimension of the driving component was 25 × 26 × 30.2 mm and the gross weight was 8.3 g, not including the battery.

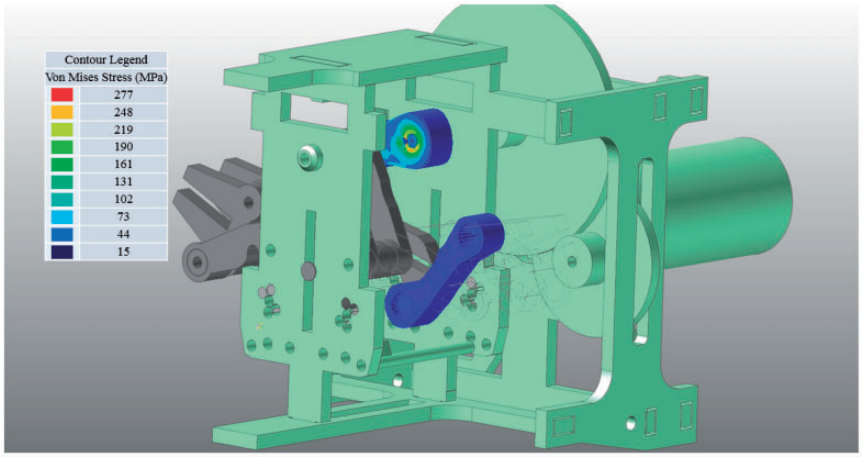

Figure 18. Result contour of Link 1 as predicted by RecurDyn.[10]

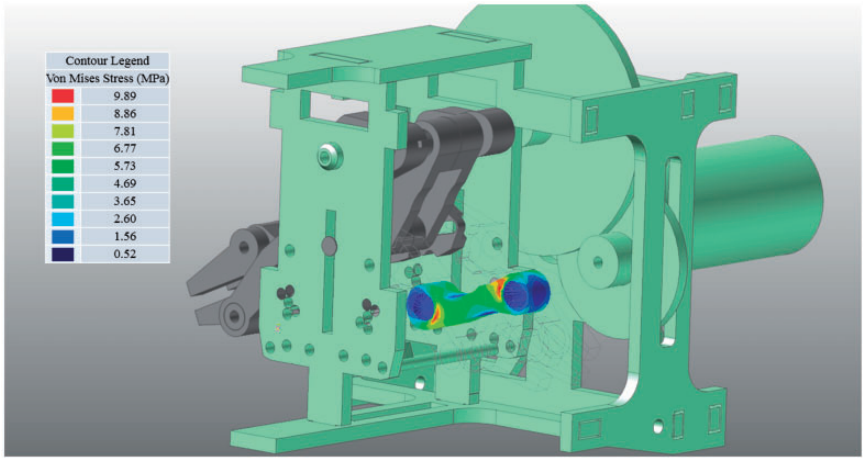

Figure 19. Result contour of Link 5 as predicted by RecurDyn.[10]

The flapping wing had a wingspan of 150 mm, and its wing membrane was made of polyethylene with a thickness of 15 microns. To support the wing, a 1 mm carbon rod was used at the leading edge of each wing. The membrane did not adhere to the carbon rod but instead enclosed the rod. Thus, when the FWMAV is in the flapping condition, the wing membrane rotates freely along the leading edge according to the inertia of the wing.

The total span is 150 mm and the weight is 8.3 g. These values are slightly smaller than those of Nano Hummingbird, which are 158 mm and 8.88 g, only including the main motor, flapping mechanism, wings and structure.[3]

During the fabrication of the control mechanism, the control joints were fixed at the control locations to implement each different control input, as depicted in Figure 8. Hence, four different types of the prototypes were fabricated in order to implement each control for neutral, positive pitch, roll and yaw.

Experiment

Using the fabricated prototype, the flapping wing trajectory was evaluated. The trajectory was measured by a high-speed camera, the Micro M100 by Phantom. In order to measure the amount of the flapping angle in the wing, each frame was analyzed to find out the peak-to-peak postures. In the test, the input voltage to supply the power was 4 V. It generated a flapping frequency of 23 Hz. The present mechanism was fixed on an extra mount, as shown in Figure 21. The first condition was the neutral condition, as shown in Figure 22(a). The flapping trajectory appeared to be symmetric, and the relevant flapping amplitude α was approximately 160°. Subsequently, by following each joint location,

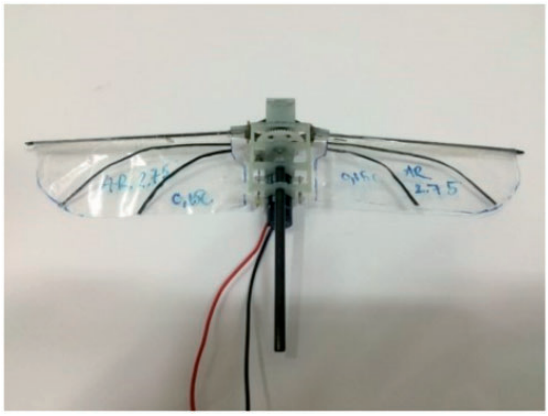

Figure 20. Assembled prototype.

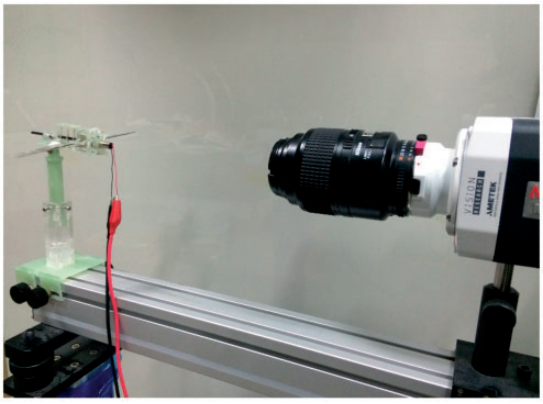

Figure 21. Flapping motions captured by the high-speed camera.

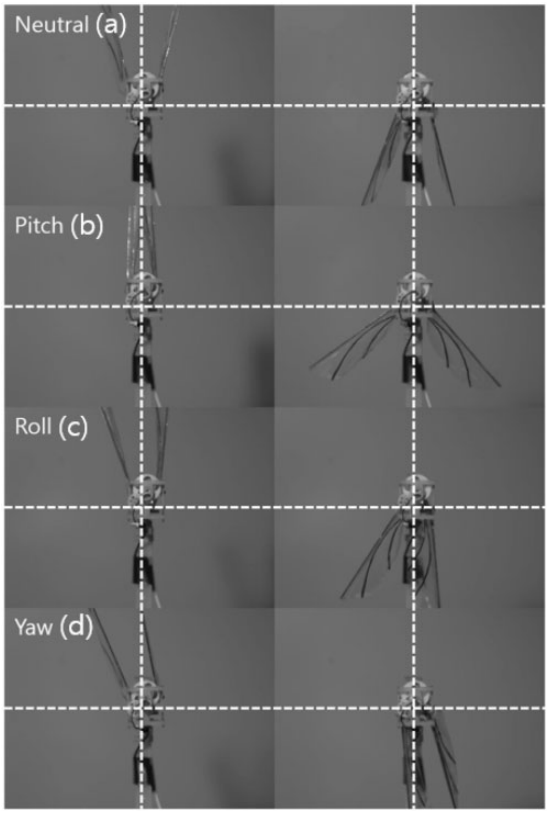

Figure 22. Fabricated prototype.

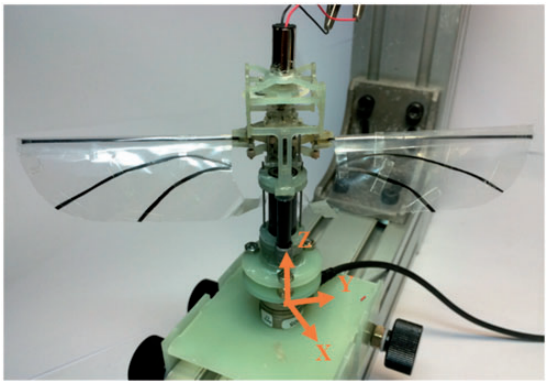

Figure 23. Fabricated test bed and load cell.

the three cases of flapping trajectories, i.e. pitching, rolling, and yawing motions, were tested. The position of each joint was based on the specifications described in Control mechanism section. The second condition was the pitching motion. The centerline of the both wings was rotated symmetrically by 8°. This motion was in good agreement with the analytical solution, as shown in Figure 22(b). The third condition was the rolling motion. For the rolling motion, from the analytical estimation, one side of the wings was 176° while the other side was 144°. As shown in Figure 22(c), these values were also in good agreement with the experiment results. The final condition was the yawing motion. It also matched the analytical solution well, as shown in Figure 22(d). In all of the conditions, there were differences of approximately ±5° between the analytic solution and the experimental results. There are several possible reasons for such differences. First, in the actual experiment, there was additional aerodynamic force on the wing surface, but it is not considered in the multi-flexible body dynamic analysis. Second, there were manufacturing inaccuracies which were generated by the CNC cutting machine or abrasions created during the fabrication procedures.

A FWMAV must change its wing aerodynamic force in order to control its position or its fuselage attitude. To validate the control capability of the FWMAV here, a test bed was created. A Nano-17 load cell by ATI was used to measure the force and moment components generated by the modification of the wing kinematics.

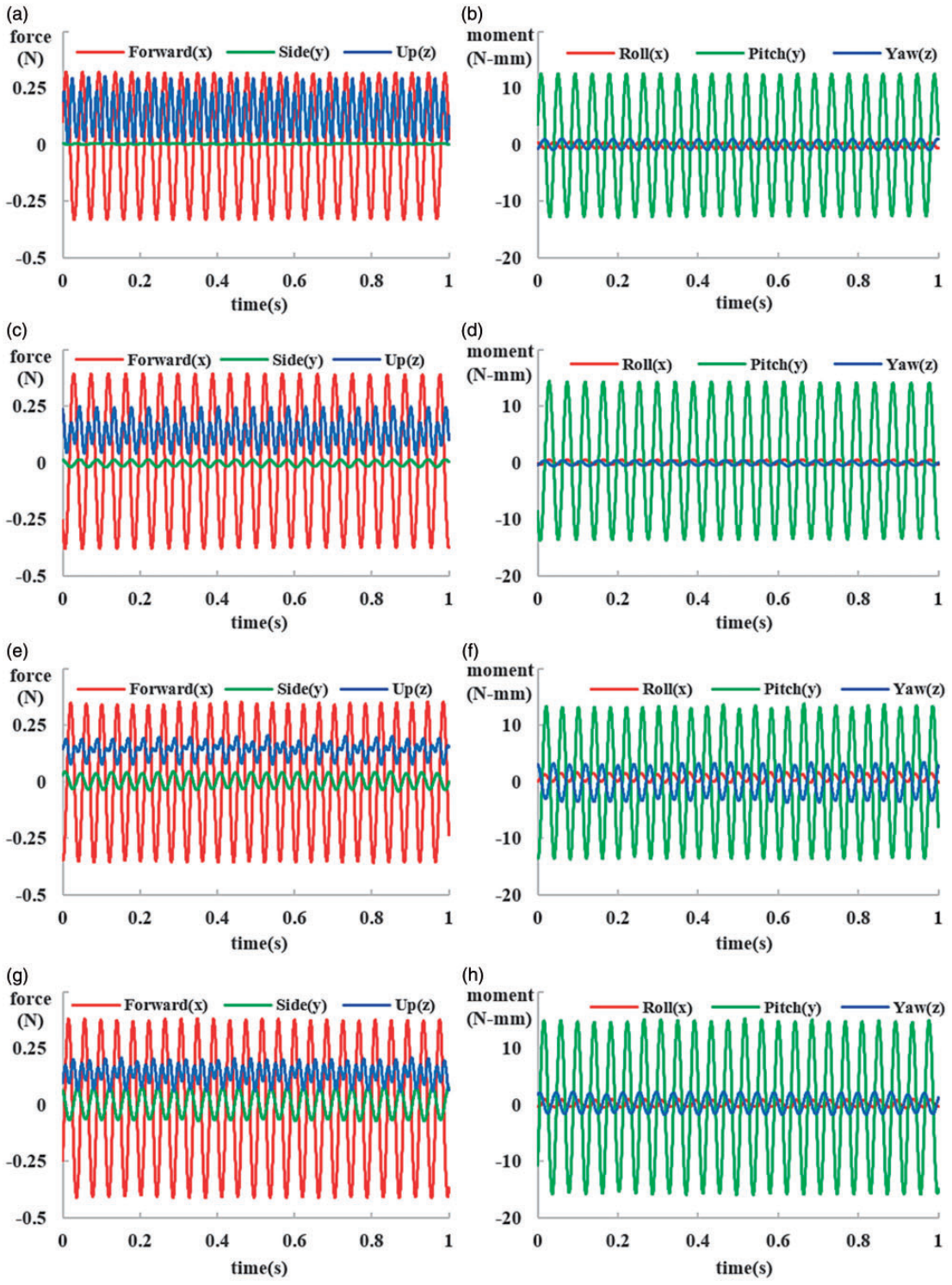

Figure 24. Quasi-steady responses for 1 s for each control input: (a) Force response for the neutral condition, (b) Moment response for the neutral condition, (c) Force response for the pitch control, (d) Moment response for the pitch condition, (e) Force response for the roll control, (f) Moment response for the roll condition, (g) Force response for the yaw control and (h) Moment response for the yaw condition.

An experimental mount with three-axis degrees of freedom was designed. It can trim the fuselage posture to obtain a more precise result while remaining connected to both the load cell and the flapping mechanism. Figure 23 shows the flapping mechanism mounted on the test bed and load cell. During the measurement, the relevant values were transformed to those referring to the center of gravity of the mechanism by using the module included in DAQ system (DAQ Force and Torque Manual Calculation). The positive Z-axis heads vertical upward of the load cell, and Y-axis lies in the center line of the flapping plane. Figures 24 and 25 show the load components obtained. All the results were smoothed by applying a low-pass filter (cut-off frequency 50 Hz). Figure 24 presents the quasi-steady responses of the 6-DOF forces and moments for 1 s after 5–6 s of operation. Figure 24(a) and (b) shows the results for the neutral state, without any control inputs. The average value of the measured vertical load was 0.141 N. Because the mass of driving component is 8.3 g, 0.081 N is needed to hover and it is expected that the present flapping mechanism is capable of flying. Moreover, the vertical load was 67% higher than the value of other linkage flapping mechanism, which was 0.84 N at 37 Hz of frequency with same span.[9] Because the present mechanism generated more thrust at lower frequency, the efficiency of the complete system is expected to be high. However, compared with the string mechanism of Nano Hummingbird, the present linkage mechanism needs more improvement. As Nano Hummingbird can lift its total mass 19 g, the thrust is at least 0.186 N which is 32% higher than the present value. Figure 24(c) and (d) shows the response for the pitching input in the (+) direction, which is (+Y) rotation. The measured average pitching moment was 0.282 N-mm. Next, the rolling moment in the + direction (+X rotation) was measured. The generated rolling moment was 0.75 N-mm, as shown in Figure 24(e) to (f). This value corresponds to the average rolling moment. The last quantity measured is the yawing moment. During the yawing motion, both wing planes were rotated in the same direction,

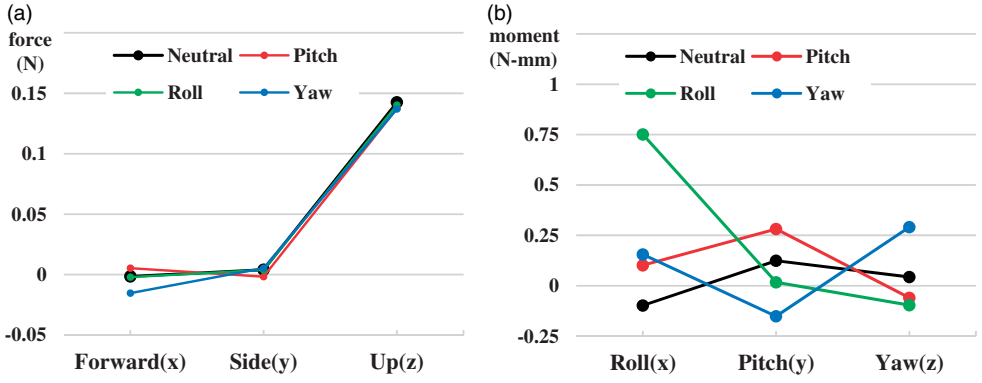

Figure 25. Mean components for each control input. (a) Mean force component for each control input. (b) Mean moment component for each control input.

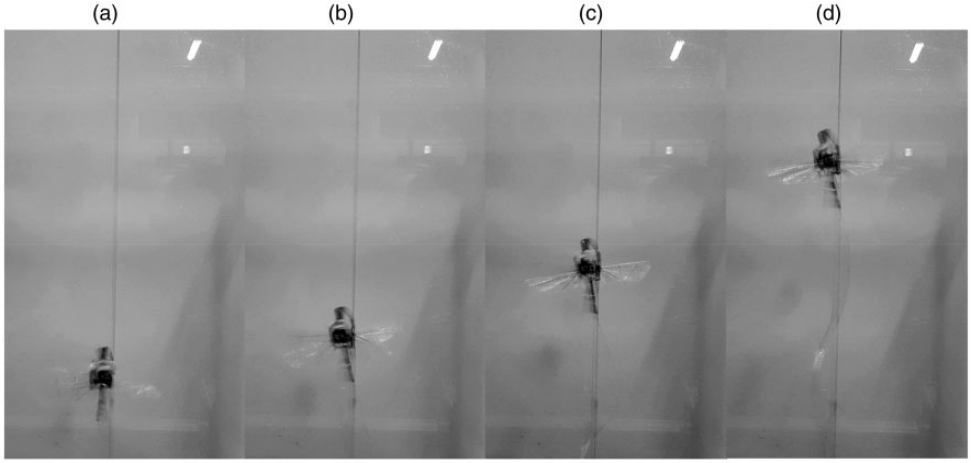

Figure 26. Guided vertical takeoff experiment. (a) t=0 s, (b) t≈2 s, (c) t≈3.5 s, and (d) t≈5 s.

either clockwise or anticlockwise. By this motion, the yawing moment was generated. The average value of the yawing moment was 0.29 N-mm. These mean values were compared in Figure 25 to evaluate the coupling between the control inputs. In Figure 25(a), the control inputs did not change the lift significantly, while the x-direction force was varied a little. In Figure 25(b), at the neutral condition, small amounts in three moment components were induced due to inaccurate fabrication or wrong estimation of the gravity center. And for each control input, certain moment component became increased, almost twice larger than the remaining moments. Thus, it is concluded that coupling between control inputs is negligible. In this experiment, the amounts of control force and moment generated by the present flapping mechanism were measured and examined. As a result, it was confirmed that the control forces and moments would be generated independently to adjust the fuselage attitude in the proposed vehicle.

To confirm the generated lift of the flapping mechanism, a vertical takeoff experiment was conducted, as shown in Figure 26. The input voltage of the supplied power was 4 V, generating a flapping frequency of 24 Hz. In this experiment, the flapping mechanism consists of only the driving components, not including therefore the battery or control system. This test focused on only the vertical thrust. Thus, the flapping fuselage was guided with iron string, which was connected to the experimental mount. In the flapping mechanism, a brass bearing was used to minimize the friction between the string and the flapping fuselage frame. The diameter of the strong was 1 mm and its length was 100 mm. Each end was fixed strongly to the experimental frame. This constrained the vertical direction motion of the present flapping mechanism. The direction of the stroke plane is identical to the horizontal plane, as shown in Figure 26. The result showed that the flapping mechanism could make sufficient vertical thrust. When the input voltage is supplied, the flapping frame will move upward. This suggests that the flapping mechanism can generate enough lift for takeoff.

Conclusion

In this paper, a new FWMAV was designed from the conceptual design stage. First, several design requirements were established using UBET. In keeping with these requirements, a detailed design of the flapping mechanism was done. For the flapping mechanism, a six-bar linkage was used, and it was expected to have a sufficient flapping stroke amplitude of approximately 160°. The total span and the weight were slightly smaller than those of Nano Hummingbird, which is expected to be advantages for FWMAV. The control mechanism was then considered to generate the flight control moment for pitching, yawing, and rolling motions. This control motion was implemented via a combination of motions by joints. The present control mechanism using the joint motion induces the motion difference between the two wings. As a result, the vehicle is capable of changing two wings' aerodynamic forces. The present concept is an integrated form of both flapping and control mechanism, which will be beneficial for the design of a small-sized tailless MAV. However, the present mechanism becomes structurally more complicated to fabricate than the other existing link mechanisms. A three-dimensional model was then created to consider the actual components and materials. To confirm the performance of the proposed design, a multi-body dynamic analysis was conducted using RecurDyn. In the analysis, the flapping amplitude was predicted to be approximately 160°. The control motion for changing the wing kinematics was also predicted by considering the joint motion along with variations of this motion. Then, the three-dimensional CAD drawings were created. Finally, the performance of the present design was evaluated in an experiment. The wing trajectory was captured by a high-speed camera. This procedure made it possible to estimate the performance of the mechanism and the fabrication error. The results were in good agreement with kinematic analysis to within $\pm 5°$. An experiment using a load cell was conducted to evaluate whether or not the generated amounts of moment could allow takeoff or proper changes of the vehicle attitude. The measured lift was much greater than that of the other linkage mechanisms, but much smaller than that of the string mechanism. It was found that the friction between the links needs to be reduced for improved efficiency. The measured pitching, rolling and yawing moments demonstrated the possibility of the control capability of the designed mechanism. However, fabrication based on this concept was undesirable, since internal and external loads were not considered. Thus, flexible multi-body dynamic analysis will be conducted by considering aerodynamic loads induced by the wing motion. In addition, the actuation mechanism controlling the joints will be designed. A comparison between the joint steering mechanism and trailing edge control mechanism which is also in progress, will deduce the proper control mechanism for the present six-bar linkage FWMAV. As a result, a detailed design of the FWMAV will be improved. Moreover, the free flight test using the present mechanism will be conducted. Especially, vertical takeoff will be examined in order to figure out the potential problem regarding the balance of the vehicle by using the presently equipped device, i.e. high-speed camera.

Acknowledgement

The authors thank Prof. HoonCheol Park at Konkuk University for providing the UBET analysis program.

Declaration of conflicting interests

The author(s) declared no potential conflicts of interest with respect to the research, authorship, and/or publication of this article.

Funding

The author(s) disclosed receipt of the following financial support for the research, authorship, and/or publication of this article: This research was supported by a grant to Bio-Mimetic Robot Research Center Funded by Defense Acquisition Program Administration, and by Agency for Defense Development (grant no. UD130070ID) and also by the program of Development of Space Core Technology through the National Research Foundation of Korea funded by the Ministry of Science, ICT, and Future Planning (grant no. NRF-2015M1A3A3A05027630).

References

1. Nguyen QV, Park HC, Byun DY, et al. *Recent progress in developing a beetle-mimicking flapping-wing system*. World Automation Congress (WAC), IEEE, 2010, pp.1–6.
2. George RB, Colton B, Mattson CA, et al. A differentially driven flapping wing mechanism for force analysis and trajectory optimization. *Int J Micro Air Vehicle* 2012; 4: 31–49.
3. Keenon M, Klingebiel K, Won H, et al. Development of the Nano Hummingbird: a tailless flapping wing micro air vehicle. In: *50th AIAA Aerospace Sciences meeting including the new horizons forum and aerospace exposition*, Nashville, Tennessee, 9–12 January 2012, p.15.
4. Teoh ZE, Fuller SB, Chirarattananon P, et al. A hovering flapping-wing micro robot with altitude control and passive upright stability. In: *IEEE/RSJ international conference on intelligent robots and systems*, Vilamoura, Algarve, Portugal, 7–12 October 2012.
5. Yang L-J. The micro-air-vehicle golden snitch and its figure-of-8 flapping. *J Appl Sci Eng* 2012; 15: 197–212.
6. Yang L-J, Esakki B, Chandrasekhar U, et al. Practical flapping mechanisms for 20 cm-span micro air vehicles. *Int J Micro Air Vehicle* 2015; 7: 181–202.
7. Festo AG. BionicOpter. April 2013, https://www.festo.com/net/SupportPortal/Files/248133/Festo_BionicOpter_en.pdf (retrieved 24 January 2017).
8. Karasek M, Nan Y, Lalami M, et al. Pitch moment generation and measurement in a robotic hummingbird. *Int J Micro Air Vehicle* 2013; 5: 299–309.
9. Truong QT, Nguyen QV, Truong VT, et al. Effect of wing twisting on aerodynamic performance of flapping wing system. *AIAA J* 2013; 51: 2013.
10. FunctionBay, Inc. Recurdyn. 2016. http://functionbay.co.kr/pdf/brochure_e_web.pdf (retrieved 24 January 2017).
11. Ansari SA, Knowles K and Zbikowski R. Design study of insect-like flapping wings in the Hover. Part II: Effect of wing geometry. *J Aircraft* 2008; 45: 1976–1990.